In-plane homogeneity and lipid dynamics in tethered bilayer lipid membranes (tBLMs)

Siddharth Shenoy,[a] Radu Moldovan,[a] James Fitzpatrick,[b] David J. Vanderah,[c] Markus Deserno[a] and Mathias Lösche*[ad]

Received 25th September 2009, Accepted 18th December 2009
First published as an Advance Article on the web 25th January 2010
DOI: 10.1039/b919988h

Tethered bilayer lipid membranes (tBLMs) were prepared by the self-assembly of thiolated lipidic anchor molecules on gold, followed by phospholipid precipitation *via* rapid solvent exchange. They were characterized by their in-plane structure, dynamics and dielectric properties. We find that the in-plane homogeneity and resistivity of the tBLMs depend critically on a well-controlled sample environment during the rapid solvent-exchange procedure. The in-plane dynamics of the systems, assessed by fluorescence correlation spectroscopy (FCS) as the diffusivity of free, labeled phospholipid dissolved in the membrane, depend on the density of the lipidic anchors in the bilayer leaflet proximal to the substrate as well as on details of the molecular structure of the anchor lipid. In DOPC tBLMs in which tethers are laterally dilute (sparsely tethered bilayer lipid membranes, stBLMs), measured diffusivities, $D \approx 4\ \mu m^2\ s^{-1}$, are only slightly greater than those reported in physisorbed bilayers (M. Przybylo, J. Sýkora, J. Humpolíckova, A. Benda, A. Zan and M. Hof, *Langmuir*, 2006, **22**, 9096–9099). However, when we distinguish label diffusion in the proximal and in the distal bilayer leaflets, we observe distinct diffusivities, $D \approx 2\ \mu m^2\ s^{-1}$ and $7\ \mu m^2\ s^{-1}$, respectively. The value observed in the distal leaflet is identical to that in free membranes. stBLMs completed with phytanoyl lipids (DPhyPC) show consistently lower label diffusivity than those completed with unsaturated chains (DOPC). As the length of the tether chain increases, a reduction in the apparent diffusivity is observed, which we interpret as an increased propensity of the proximal bilayer leaflet to host free lipid. We also investigated preparation conditions that control whether the tBLMs are laterally homogeneous, as assessed by optical microscopy. In laterally heterogeneous bilayers, the label diffusivity varies only by a factor of ~2 to 4, indicating that the regions in the bilayers with different label solubilities do not correspond to distinct phases, such as a fluid phase coexisting with a gel phase.

I. Introduction

Lipid membranes separate the interior space of cells from the outside world and compartmentalize the cytoplasm into organelles. Because both internal membranes and the plasma membrane reorganize in response to many external and internal stimuli, membrane fluidity is of crucial importance for the functioning of the cell. However, the high biochemical complexity of cells and cell organelles makes *in vivo* molecular-scale characterizations of structure and interactions extremely difficult. Therefore, the quest to make basic molecular interactions accessible to physical characterization has driven the development of synthetic biomimetic membranes.[1,2]

Among the different model membranes that have been developed, solid supported membranes[3] are particularly robust and are amenable to many physical characterization techniques due to their planar geometry. They are easily prepared by vesicle fusion[4] and conveniently studied with tools such as fluorescence microscopy,[5] X-ray or neutron reflection[6] for structural characterization while techniques such as surface-plasmon resonance (SPR)[7] are frequently used to quantify molecular interactions that occur at such membranes. Because of their simple geometry, electrochemical characterization techniques, such as electrochemical impedance spectroscopy (EIS),[8] can be quantitatively evaluated to study electrical properties of the membrane. For example, it is straightforward to quantify the dielectric constant, ε, of the hydrophobic interior of the bilayers by a combination of EIS and neutron reflectometry.[9]

To control the interface between the membrane and its inorganic support better, polymer-supported as well as chemically tethered membranes have more recently been devised.[6,10,11] In such systems, a nanometre thick hydrated layer between the substrate and the bilayer leaflet proximal to the substrate is stabilized by a hydrophilic polymer, thus preventing physisorption of lipid on the substrate. While this separation is achieved by adsorbing the bilayer onto an ultrathin polymer network to form polymer-supported membranes,[12] tethered bilayer lipid membranes (tBLMs) employ lipidic anchor molecules which attach covalently to the substrate, span the hydrated space with a short hydrophilic chain (tether) and bind the membrane to the solid support by incorporating into the bilayer

[a]*Physics Department, Carnegie Mellon University, Pittsburgh, PA, USA. E-mail: quench@cmu.edu; Fax: +1 412 268 8252; Tel: +1 412 268 8367*
[b]*Molecular Biosensor and Imaging Center (MBIC), Carnegie Mellon University, Pittsburgh, PA, USA*
[c]*Chemical Sciences and Technology Laboratory, National Institute of Standards and Technology, Gaithersburg, MD, USA*
[d]*Center for Neutron Research, National Institute of Standards and Technology, Gaithersburg, MD, USA*

with their hydrophobic chains.[6] It has been shown that such tBLMs are stable in their dielectric properties over the course of months.[13] Not surprisingly therefore, tBLMs prepared from synthetic phospholipids are increasingly being used to mimic biomembranes in studies of protein reconstitution[14–18] and of enzyme[19] or peptide interaction[9,20] with membranes. In such applications it is desirable that the lipid matrix remains fluid in order to accommodate the proteins in a biomimetic environment. Low-melting phospholipids, such as DOPC or DPhyPC (dioleoyl or diphytanoyl phosphatidylcholine, respectively) are often used for tBLM formation to achieve this goal. An example is the recent characterization of the exotoxin, α-hemolysin from *Staphylococcus aureus*, in tBLMs.[15]

In a preparation strategy that we have recently developed to form tBLMs, the lipidic anchors are chemisorbed as a pure compound from ethanolic solutions, resulting in the formation of a self-assembled monolayer (SAM). In a second step, the bilayer is completed by rapid solvent exchange[1,6] resulting in the precipitation of phospholipids onto the SAM. The resulting membrane incorporates the anchors in its layer proximal to the substrate. In this case, the proximal leaflet consists entirely of anchor molecules, *i.e.*, it contains no, or minimal, free phospholipid. We will refer to such systems as densely tethered bilayer lipid membranes (dtBLMs). As a variation of this general strategy, tethers can be laterally diluted by coadsorption of the anchor molecules with a hydrophilic backfiller, such as β-mercaptoethanol (βME), that results in the formation of a mixed SAM. Rapid solvent exchange then leads to the formation of a sparsely tethered bilayer lipid membrane (stBLM). It has been demonstrated that stBLMs are a better option for protein reconstitution[15] than dtBLMs,[21] presumably because of a higher flexibility of the membrane due to the presence of free phospholipid in the proximal layer.

By varying the chemical architecture of the lipidic anchor molecules, the properties of the resulting interface architecture can be further fine-tuned.[22] In this paper, we report on the dynamic properties of free phospholipids, as studied with fluorescence correlation spectroscopy (FCS),[23–25] comparing two different anchor molecules, termed WC14[6] and FC16,[22] in dtBLMs and stBLMs. Fluorescence microscopy (FM) is employed to study in-plane structure as a function of the preparation procedure and correlate optical heterogeneity with electrical properties. Because DPhyPC and DOPC tBLMs are frequently used in studies of protein–membrane interactions, we explored in this work conditions that lead to homogeneous bilayers in tBLMs composed of these lipids, and have characterized their in-plane dynamics.

II. Materials and methods†

1. Materials

The 1-thiaoligo(ethylene oxide) dialkyl lipids, WC14 and FC16, were synthesized, purified and characterized as described earlier.[6,22] β-Mercaptoethanol (βME) was purchased from Sigma-Aldrich, St Louis, MO, and distilled before use. The phospholipids DOPC, DPhyPC, LR-DOPE (1,2-dioleoyl-*sn*-glycero-3-phosphocholine, 1,2-diphytanoyl-*sn*-glycero-3-phosphocholine and 1,2-dioleoyl-*sn*-glycero-3-phosphoethanolamine-*N*-[lissamine rhodamine B sulfonyl], respectively) were used as supplied from Avanti Polar Lipids (Alabaster, AL). Ultrapure H_2O was obtained from a Millipore (Billerica, MA) UHQ reagent grade water purification system. Potassium iodide (99.995% pure) was from Acros Organics (Morris Plains, NJ).

2. tBLM preparation

Three inch [100] cut Si wafers (thickness, $d = 380\ \mu m \pm 25\ \mu m$; Silicon Quest Intl., Inc., Santa Clara, CA) were cleaned in two steps: gently wiping with Hellmanex solution (Hellma GmbH, Müllheim, Germany) and immersion in Nochromix solution for 15 min. (Godax Laboratories, Inc., Cabin John, MD). Both steps were followed by copious rinsing with water. The cleaned wafers were coated with Cr (~10 Å) and Au (~450 Å) films by high-energy magnetron sputtering (ATC Orion, AJA Intl. Inc., North Scituate, MA). The deposition parameters have been optimized and shown to result in surfaces of the gold film that are smooth over large areas with an rms. roughness of <5 Å.[6] Immediately after breaking the vacuum, the coated wafers were transferred into 0.2 mM ethanolic solutions of pure WC14, FC16, or binary mixtures of these compounds with βME at molar ratios of 30 : 70. After overnight incubation, the wafers were rinsed with absolute ethanol and dried with nitrogen. Depending on βME content, the SAM-coated wafers show static wetting contact angles with water of 80–108°.[22] Splinters were cut from the SAM-coated wafers (5 mm × 5 mm for fluorescence microscopy and correlation spectroscopy measurements and 20 mm × 40 mm for electrochemical impedance spectroscopic characterization). tBLMs were completed by exposing the SAM-coated splinters to a concentrated phospholipid solution (10 mg mL^{-1} DOPC or DPhyPC), followed by the rapid replacement of this solution by aqueous buffer (100 mM NaCl, 10 mM NaH_2PO_4, pH 7.4).[1]

3. Sample characterization

tBLMs labeled with LR-DOPE were characterized with fluorescence microscopy (FM). To correlate in-plane texture with electrical characteristics of the bilayer, we conducted electrochemical impedance spectroscopy (EIS) followed by FM imaging of the samples. In distinct experiments, we imaged labeled tBLMs with laser scanning microscopy (LSM) followed by fluorescence correlation spectroscopy (FCS) performed on selected spots of these samples. Henceforward, these experiments are denoted as "EIS/FM" and "FM/FCS", respectively. For FM or FM/FCS experiments, the rapid solvent exchange was performed by introducing the 5 × 5 mm^2 splinters into a Nunc Lab-Tek chambered cover glass (Thermo Fisher Sci., Rochester, NY) sample cell, where they rested without fixation. For EIS/FM experiments, 20 mm × 40 mm splinters were mounted on the bottom of a Teflon (PTFE) EIS sample holder that separates 6 electrochemical cells, each with a cross-section of $A \approx 0.33\ cm^2$ and a fluid volume $V \approx 300\ \mu L$ for EIS measurements and then

† Certain commercial materials, pieces of equipment, and instruments are identified in this manuscript in order to specify the experimental procedure as completely as possible. In no case does such identification imply a recommendation or endorsement by the National Institute of Standards and Technology, nor does it imply that the materials, equipment, or instruments identified are necessarily the best available for the purpose.

transferred under buffer into a Nunc Lab-Tek single-chamber cover glass sample cell for FM imaging. Phospholipids were doped with 0.06 mol% and 0.003 mol% LR-DOPE for EIS/FM and FM/FCS experiments, respectively. All preparation steps and sample characterization measurements (see below) were performed at room temperature ($T = 21 \pm 1$ °C).

Electrochemical impedance spectroscopy (EIS). EIS was performed with a Solartron 1287A potentiostat and a 1260 frequency analyzer (Farnborough, UK). Au-coated silicon wafers (20 mm × 40 mm) served as the working electrode in the electrochemical cells in which the surface areas on the Au film were defined by Viton O-rings. Copper contrast was used to measure the geometric electrode surface area, and the raw EIS data were normalized to these areas. A saturated silver–silver chloride microelectrode served as the reference (Microelectrodes, Bedford, NH, model M-401F). The auxiliary electrode was a 0.25 mm diameter Pt wire (99.99% purity, Aldrich) coiled around the barrel of the reference electrode. The distance between the tip of the reference and working Au electrode surface was set to 2–3 mm. Measurements were carried out with 10 mV ac at 0 V bias *vs.* the reference electrode in aerated solutions.

EI spectra were normalized to the sample surface area and fitted to equivalent circuit models (ECMs) as previously described[6] using ZView (Scribner Associates, Southern Pines, NC). The ECM used here is shown in Table 1 and was discussed in more detail in earlier work.[6,19] Confidence limits for the fitted parameters were quantified through the variance–covariance matrix estimate of the Levenberg–Marquardt χ^2 minimization.

Fluorescence microscopy (FM). FM was performed on two commercial Zeiss microscopes (Carl Zeiss, Jena, Germany): an Axiotech^{vario} epifluorescence microscope fitted with an EM-CCD mod. C9100 video camera (Hamamatsu Photonics, Herrsching, Germany) and a confocal microscope LSM 510 Meta, described in more detail below. On the Axiotech^{vario}, a Zeiss filter set (excitation: BP 510–560, beam splitter: FT 580, emission: LP 590) was used to image the lateral distribution of LR-DOPE through a Zeiss Water Achroplan (20 × 0.5 NA) objective lens.

Fluorescence correlation spectroscopy (FCS) instrumentation. Two different setups were used for FCS correlation experiments: the confocal LSM 510 Meta, in which chromophores are excited at the fundamental frequency of the excitation beam ("one-photon" or "1P" microscopy) and a frequency-doubled system of local design ("two-photon" or "2P" microscopy). The 1P microscope was used for assessing sample homogeneity and characterizing differences in label diffusivity where tBLMs were inhomogeneous. More extensive diffusion measurements of tBLM samples for which homogeneity on the optical length scale was previously established with FM on the Axiotech^{vario} or the 1P FCS microscope were then performed on the 2P FCS instrument. Although the 2P instrument does not offer imaging capabilities, it is optimized for characterization of dynamic properties of biological and biomimetic samples.

1P FCS setup. The LSM 510 Meta employs a Confocor 3 detection module mounted on an Axio Observer Z1 inverted microscope frame (Carl Zeiss). Excitation light is provided at a wavelength, $\lambda = 561$ nm by a diode-pumped solid state (DPSS) laser attenuated *via* an acousto-optical tunable filter (AOTF). Typical powers at the rear pupil of the objective lens were 10–20μW. Excitation light was coupled into the 40 × 1.1 NA LD-C-Apochromat water immersion objective, which was corrected for coverslip thickness (0.14–0.18 mm), *via* the LSM 510 scan head module. Fluorescence emission is epi-collected through the objective and directed to the Confocor 3 module where it is detected by a single fiber-coupled avalanche photodiode (SPCM-AQR14, Perkin-Elmer, Fremont, CA) mounted behind a 575–615 nm bandpass filter (Semrock, Rochester, NY). Photon counts from the detector were subsequently processed and auto-correlation functions (ACFs) and photon counting histograms calculated on the fly using the ZEN software (Carl Zeiss).

2P FCS setup. The two-photon FCS system is based on an Axiovert 200M inverted microscope frame (Carl Zeiss) with infrared excitation light from a Mira 900F mode-locked titanium sapphire laser (125 fs pulse width, 76 MHz repetition rate) pumped by a 10 W continuous wave DPSS laser operating at $\lambda = 532$ nm (Verdi V10, Coherent, Santa Clara, CA). The titanium sapphire laser provides an output wavelength range between 700 and 980 nm. Its power output in the mode-locked regime averages 1.8 W at $\lambda = 780$ nm. A neutral density (ND) filter wheel in the primary beam path serves to reduce the intensity of the infrared excitation light to 5–10 mW before entering the microscope *via* a custom-made entrance on the side of the reflector turret. Once entered into the turret, the attenuated infrared excitation light is directed up to the objective *via* a dichroic mirror (750dcspxr, Chroma Technologies, Rockingham, VT). The objective used for all FCS measurements was a 63 × 1.2 NA C-Apochromat water immersion lens (Carl Zeiss) corrected for coverslip thickness (0.14–0.18 mm). Fluorescence excited *via* two-photon excitation is epi-collected and passed through an additional bandpass filter (et575/50m-2p, Chroma Technologies, Rockingham, VT) providing additional infrared rejection above 700 nm to remove stray light passing through the dichroic mirror that might otherwise reach the photodetectors. The fluorescence is first focused *via* the microscope tube lens and then re-collimated *via* an achromatically corrected doublet lens, reaching a 50 : 50 beam splitter cube (Thorlabs, NJ) which splits the light into two beams. These beams are focused *via* two achromatically corrected doublet lenses onto the active surface areas of two separate avalanche photodiode detectors (SPCM-AQR14, Perkin-Elmer, Fremont, CA). Photon counts from each detector are then sent to a hardware correlator (5000EPP, ALV, Langen, Germany) which calculates the ACF.

FCS data acquisition by sample scans through the focal plane (z-scan FCS). FC spectra reported here consist typically of the average of two runs, each of 2 min length in 2P FCS measurements and of the average of 10 runs of 20 s each in 1P FCS measurements. The ACF of the emission of a single labeled species due to a diffusion process that is confined to a narrow layer (lipid bilayer thickness, $d \approx 5$ nm $\ll \lambda$) within a Gaussian excitation volume has the form:[26]

$$G_{2D}(\tau) = \frac{1}{\langle N \rangle} \frac{1}{1 + \tau/\tau_D} \quad (1)$$

τ is the time differential between two points in a time sequence, $<N>$ is the time-averaged number of fluorescent molecules diffusing through the light volume and τ_D is their characteristic diffusion time. An anomalous diffusion correction, $(1 + \tau/\tau_D) \rightarrow (1 + \tau/\tau_D)^{\alpha}$, was always considered in the data evaluation. However, we found that the measured ACFs were always consistent with regular diffusion as long as tBLMs were located close to the beam waist when scanning the focus across the sample (see below). The ACF of a two-dimensional (2D) diffusion process is a simplified form of the 3D equivalent,[27]

$$G_{3D}(\tau) = \frac{1}{\langle N \rangle} \frac{1}{1 + \tau/\tau_D} \frac{1}{\sqrt{1 + (\tau/\tau_D)(r_o^2 z_o^2)}} \quad (2)$$

(where r_o and z_o refer to the extension of the focal volume into the radial and normal directions, respectively, with respect to the focal plane). To evaluate $G_{2D}(\tau)$ quantitatively, N and τ_D are obtained from fitting eqn (1) to an individual ACF. However, the validity of eqn (1) depends on the membrane being precisely located in the focal plane of the microscope (Fig. 1): only if the sample is located at $z = z_o$ (Fig. 1) is there a simple connection between the measured value of τ_D and the diffusion constant D:

$$\tau_D = \frac{r_o^2}{4D} \quad (3)$$

If measurements are taken at $z = z_o + \Delta z$, the sample is still illuminated by a Gaussian beam profile, but the beam cross-section in the confocal geometry increases as[28]

$$r^2 = r_o^2 \left(1 + \frac{\lambda^2 \Delta z^2}{\pi^2 n^2 r_o^2}\right) \quad (4)$$

(where n is the refractive index of the medium and λ is the laser wavelength in vacuum) and τ_D changes accordingly as[25]

$$\tau_D(1P) = \frac{r_o^2}{4D}\left(1 + \frac{\lambda^2 \Delta z^2}{\pi^2 n^2 r_o^4}\right) \text{ or } \tau_D(2P) = \frac{r_o^2}{8D}\left(1 + \frac{\lambda^2 \Delta z^2}{\pi^2 n^2 r_o^2}\right) \quad (5)$$

for 1P or 2P microscopy, respectively. The difference in the prefactors originates from distinct optical convolution factors which involve a squared Gaussian in 1P, due to the presence of the pinhole, but a (single) Gaussian in 2P microscopy.[29] Measurements of $G_{2D}(\tau,z)$ for multiple locations, z, around the true focal plane are used to determine $z = z_o$ from the minimum of $|_D(z)$ in eqn (5).[25]

4. Diffusion measurements that discriminate the two distinct monolayers of the tBLM

A measurement of LR-DOPE fluorescence correlation in an stBLM reports dynamic properties indiscriminate of whether a label is located in the proximal or distal monolayer leaflet. However, dynamic properties of the phospholipids in these two leaflets may be significantly different due to the immobilization of the tether lipids which reside exclusively in the proximal leaflet. In order to discriminate the fluorescent signals coming from the two leaflets we performed measurements on dtBLMs

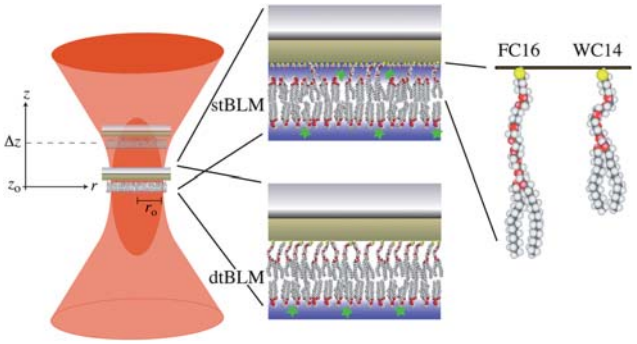

Fig. 1 Left: sample placement within the beam focus in the FCS experiment. The sample consists either of a sparsely tethered bilayer lipid membrane (stBLM, top right), in which the lipid layer proximal to the substrate is interspersed with free phospholipid and therefore also contains head group labeled LR-DOPE (stars), such that labels occur in both lipid layers. Alternatively, the sample may consist of a dtBLM (lower right), in which there is little or no free phospholipid—and therefore also no lipid label—located in the proximal leaflet. In order to determine the optimal location of the sample in the focal area, the sample is scanned along the z axis and the optical correlation function $G(\tau)$ measured for various positions Δz near $z = z_o$. For details, see text.

(tether lipid : βME = 100 : 0 in the parent SAM) where we expect no mobile phospholipids, and therefore also no label, in the proximal leaflet. In a different set of experiments, we measured FCS in stBLMs (tether lipid : βME = 30 : 70) in which potassium iodide (KI) was used as a membrane-impermeable fluorescence quencher[30] so that the fluorescent signal is expected to derive from the proximal leaflet exclusively.

5. Averaging of multiple diffusivity measurements

The lipid diffusion measurements reported below inherit two sources of error. One is variability in sample preparation, both locally in terms of micro-heterogeneity of the tBLMs and globally as there may be sample-to-sample variations. The other source of error is the uncertainty in the FCS data, estimated from the covariance matrix of Levenberg–Marquardt fits of eqn (5) to the data. Assuming that both of these sources of error are Gaussian, the average value of the diffusion constant, D, can be derived using a maximum-likelihood method (see Appendix).

III. Results

1. Fluorescence microscopic investigations of optical homogeneity

tBLMs prepared by vesicle fusion have been shown to comprise uniform bilayers if phospholipids are used that are fluid at room temperature.[31] Similarly, supported bilayers prepared on various substrates by vesicle fusion can be in-plane homogeneous,[32] which is useful for patterning or for studies of phase separation induced by chemical heterogeneities. dtBLMS and stBLMs prepared from DOPC or DPhyPC solutions by rapid solvent exchange compare well with these alternate preparations. They are uniform on the optical length scale if turbulent flow near the substrate surface is avoided in the solvent-exchange step, as shown in Fig. 2: DPhyPC on FC16–βME (30 : 70) and DOPC on

Table 1 Electrochemical characteristics of DOPC dtBLMs as determined from fitting EI spectra such as those shown in Fig. 3 to the ECM shown in the upper left. The raw data are normalized to the nominal electrode area, $A \approx 0.33$ cm^2. No roughness correction has been applied

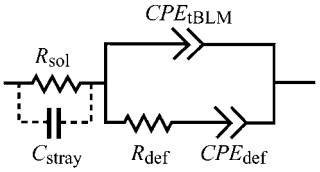

	CPE_{tBLM}/μF cm^{-2}s$^{(\alpha-1)}$	α_{tBLM}	R_{def}/MΩ cm^2	Fit quality, χ^2 ($\times 10^5$)
tBLM sample shown in Fig. 3a	0.580 ± 0.002	0.9921 ± 0.0005	1.30 ± 0.10	2.73
tBLM sample shown in Fig. 3c	0.593 ± 0.002	0.9864 ± 0.0006	0.29 ± 0.01	2.86

pure WC14 in panels (a) and (b), respectively. The micrograph shown in Fig. 2a was obtained on the LSM 510 with 0.003 mol% of LR-DOPE and has been post-processed by linearly enhancing the contrast while the image in Fig. 2b (0.06 mol% LR-DOPE) shows the raw data.

2. Correlation between optical homogeneity and electrochemical characteristics

An important characteristic of tethered bilayer systems is their resistance to ion transport across the membrane. We have extensively characterized stBLMs such as the ones investigated here with EIS in recent work[6,22] and found residual defect resistivities, derived from fits to equivalent circuit models (ECMs) such as that shown in Table 1, of $R_{def} \gg 100$ kΩ cm^2. Beyond the magnitude of R_{def}, we argued that both the constant phase element (CPE) exponent α and the length of the low-frequency tails of the complex impedance represented in Nyquist or Cole–Cole plots are metrics of bilayer quality, where $\alpha \approx 0.5$ and short low-frequency tails are consistent with near-perfect insulation properties.[6] Here we investigate the correlation of optical homogeneity of stBLMs with the appearance of EIS spectra.

Fig. 3 shows Nyquist plots of EI spectra for two independently prepared DOPC dtBLMs based upon FC16 with 0.06 mol% LR-DOPE, as well as fluorescence micrographs imaged immediately after the EIS measurements. The two dtBLMs shown were nominally prepared by following the same procedure. However, spurious differences, conceivably for example in the streaming pattern adjacent to the substrate surface during the rapid solvent exchange, frequently lead to minor differences in the electrochemical spectra of the resultant bilayers. Fig. 3 shows indeed that the bilayer which is optically more inhomogeneous (Fig. 3d) also shows an EI spectrum in which the low-frequency regime has higher values of the complex capacitance (Fig. 3c) than that (Fig. 3a) of the bilayer that shows better optical homogeneity (Fig. 3b). Note that the EI spectral range measured for both dtBLMs is identical. Table 1 shows the corresponding electrochemical parameters derived from fitting to the ECM. Optical inhomogeneity is associated with the elongation of the low-frequency tail in the EIS plot which in turn correlates with an increased electrical defect density in the bilayer.

Preparation approaches in which the flow patterns in the rapid solvent exchange are even more turbulent lead to tBLMs with

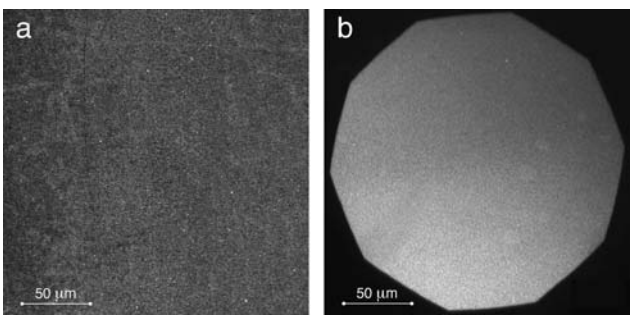

Fig. 2 Fluorescence micrographs of LR-DOPE labeled stBLMs. (a) tBLM based upon FC16/βME (30 : 70) and DPhyPC. LR-DOPE concentration is 0.003 mol% with respect to DPhyPC. The contrast in the original image has been linearly enhanced. (b) dtBLM based upon 100% WC14 SAM and DOPC. LR-DOPE concentration is 0.06 mol% with respect to DOPC. Note that the image in (a) was obtained by scanning the beam across the sample and therefore does not show an image of the field stop as seen in image (b).

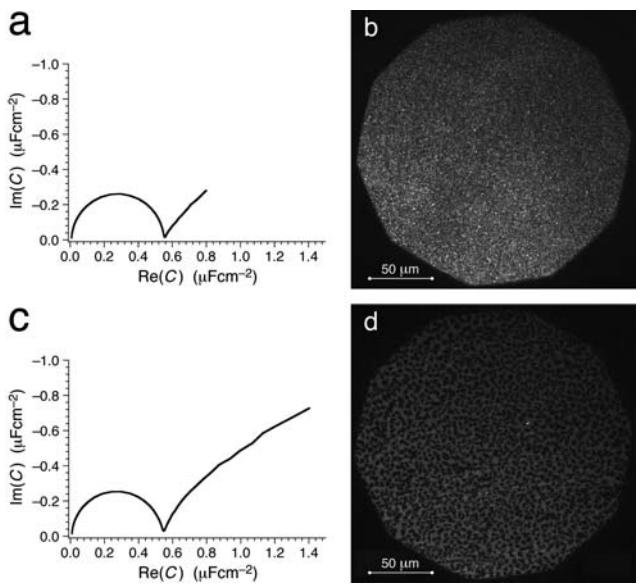

Fig. 3 EI spectra (a and c) and corresponding fluorescence micrographs (b and d) of two DOPC (0.06 mol% LR-DOPE) dtBLMs prepared on 100% FC16 SAMs (no βME spacer). Both samples were nominally identically prepared, but uncontrolled differences in the bilayer completion steps led to differences in electrochemical properties and optical homogeneity. For details see text.

optical morphologies that are reminiscent of phase-separated lipid Langmuir monolayers.[33,34] Typically, EI spectra also indicate poorer electrochemical properties (large residual defect conductivities and long low-frequency tails) for such preparations.

3. Diffusivity of LR-DOPE in tethered DOPC bilayers

Quenching of the LR-DOPE fluorescence by the nearby gold film, which has a distance to the bilayer center of ~35 Å as shown by neutron reflection,[6] is less of an issue than we had anticipated. For a comparison of the fluidity of DOPC stBLMs with that of the same lipid in free bilayers, *e.g.* in giant unilamellar vesicles (GUVs), FCS measurements were performed on a 2P microscope. On this instrument, the distribution of fluorescence labels cannot be imaged. tBLMs were prepared on SAMs from WC14 or FC16 under conditions for which an optically homogeneous distribution of the labels, such as the ones shown in Fig. 2, was previously established.

Fig. 4a shows an example of an ACF determined for the LR-DOPE fluorescence in an stBLM of DOPC on WC14/βME (30 : 70) and fitted to eqn (1). Note that due to the preparation procedure, the LR-DOPE label (0.003 mol% in DOPC) is contained in both leaflets of the bilayer. The τ_D derived from this single measurement is not a precise measure of the diffusion constant, D. Because the bilayer may be displaced along the z direction from the focal plane, the intersection area of the beam with the bilayer membrane, $A_{beam} = \pi r^2$ (Fig. 1), is not precisely known, and D can therefore not be determined from the fitted value τ_D. For an independent determination of r_o and τ_D (see eqn (5)), samples were scanned along the z axis as described by Benda and co-workers.[25] Fig. 4b shows 7 such measurements, each displaced by ~300 nm along the z axis, fitted to eqn (1).

The solid line in Fig. 4b shows the best fit to a second order polynomial (eqn (5)) through the data points of this z-scan. The values $r_o \approx 0.48$ μm and $\tau_D \approx 7$ ms associated with the minimum determine the diffusion constant, $D \approx 4.1$ μm^2 s^{-1}. To check on reproducibility and reduce statistical uncertainties, $n = 24$ z-scans on 8 independently prepared samples were conducted. Their distribution and uncertainties are shown in Fig. 4c. By accounting for their weights in a maximum-likelihood approach (see Appendix), we obtain the best estimate of the diffusivity of LR-DOPE in the DOPC stBLM based on WC14, $D = 4.1 \pm 0.1$ μm^2 s^{-1}. Similar measurement series were performed for DOPC stBLMs based on FC16, for which $D = 3.6 \pm 0.2$ μm^2 s^{-1} ($n = 14$), see Table 2. None of the ACFs obtained near $z = z_o$ showed any signature of anomalous diffusion.

We must expect that the label diffusivities are different in the two leaflets forming the bilayer, because the leaflet proximal to the substrate contains substantial amounts of the immobilized tether. Therefore, it is important to evaluate separately the diffusion constants of LR-DOPE in DOPC in these two distinct leaflets. To determine D in the distal monolayer, we performed FCS measurements on DOPC dtBLMs (prepared without βME), for which the dense spacing of the tether lipid, WC14 or FC16, prevents intercalation of free lipid, and therefore also of the lipid label, into the proximal monolayer. Conversely, to determine the label diffusivity in the proximal leaflet, FCS was also measured on stBLMs similarly prepared as those shown in Fig. 4, in which

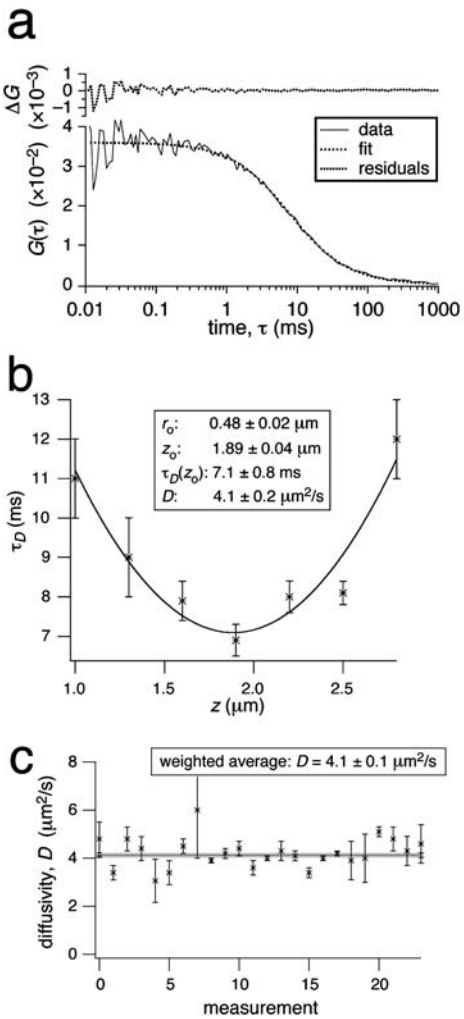

Fig. 4 FCS measurements of a DOPC stBLM on WC14/βME (30 : 70). Both leaflets in the bilayer are labeled with LR-DOPE (0.003 mol% with respect to DOPC). (a) An individual FCS measurement fitted to the 2D model, eqn (1). (b) Series of 7 FCS results in which the beam focus was shifted by ~300 nm along the z axis between measurements. Each individual ACF was evaluated using the same procedure as that in panel (a) and the associated error bars determined from the covariance matrix of the Levenberg–Marquardt fit of eqn (5) to the data. The resulting value of the diffusion constant, evaluated at z_o, is $D = (4.1 \pm 0.2)$ μm^2 s^{-1}. (c) Results from 24 independent D measurements such as that shown in panel (b), weighted by the inverse magnitude of their associated errors (see Appendix). The resulting maximum-likelihood result is $D = 4.1 \pm 0.1$ μm^2 s^{-1}. Note that there is no signature of a bimodal distribution of D values in panel (c). This suggests that the stBLM samples were laterally homogeneous, as optical heterogeneities tend to be bimodal (Fig. 3d) and we show below (Fig. 6) that the associated differences in diffusivities that are typically of the order of 2×–4×.

the buffer phase contained the fluorescence quencher potassium iodide at a concentration, $c_{KI} = 100$ mM. Fluorescence intensity measurements as a function of quencher concentration (Fig. 5a) showed that the LR-DOPE fluorescence is suppressed to the background level at this concentration. These two series of z-scan FCS measurements, on a DOPC stBLM (WC14/βME = 30 : 70) with 100 mM KI (Fig. 5b) and on a DOPC dtBLM with pure WC14 (Fig. 5c), established that the label mobility is different in

Table 2 Lipid diffusivities in stBLMs and dtBLMs. In stBLMs without quencher (columns 2 and 5), the lipid-bound label is distributed between the bilayer leaflets that are distal and proximal to the substrate. The label resides primarily in the distal layer in the dtBLM (column 4). Fluorescence emission is primarily from the proximal leaflet in the stBLM with KI quencher in the adjacent buffer phase (column 3). None of the ACFs determined near $z = z_o$ showed a signature of anomalous diffusion

Tether : βME (lipid), other condition tether lipid	30 : 70 (DOPC), sparsely tethered	30 : 70 (DOPC), 100 mM KI (inner leaflet)	100 : 0 (DOPC), densely tethered	30 : 70 (DPhyPC), sparsely tethered
WC14	(4.1 ± 0.1) μm^2 s^{-1} ($n = 24$)	(2.0 ± 0.2) μm^2 s^{-1} ($n = 14$)	(7.1 ± 0.3) μm^2 s^{-1} ($n = 17$)	(3.1 ± 0.6) μm^2 s^{-1} ($n = 5$)
FC16	(3.6 ± 0.2) μm^2 s^{-1} ($n = 14$)	n.d.	(5.4 ± 0.2) μm^2 s^{-1} ($n = 25$)	(2.5 ± 0.3) μm^2 s^{-1} ($n = 5$)

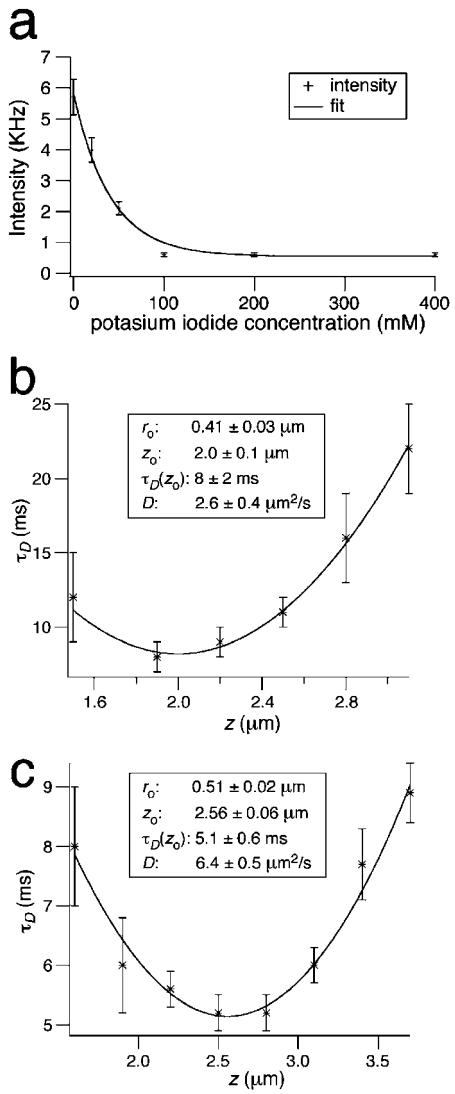

Fig. 5 (a) Fluorescence intensity from a dtBLM (DOPC on WC14 with 0.06 mol% LR-DOPE) as a function of c_{KI} in the aqueous buffer phase adjacent to the bilayer. (b and c) Series of individual FCS measurements on a DOPC stBLM and 100 mM KI in the buffer phase (panel b) and on a DOPC dtBLM (panel c), both based on WC14 and doped with 0.003 mol% LR-DOPE, in which the beam foci have been shifted along the z axis. The determined values of the diffusion constants are $D = 2.6 \pm 0.4$ μm^2 s^{-1} and $D = 6.4 \pm 0.5$ μm^2 s^{-1}.

the two bilayer leaflets with $D \approx 7.1$ μm^2 s^{-1} in the distal monolayer and $D \approx 2.0$ μm^2 s^{-1} in the proximal monolayer. We are aware that KI might affect the lipid mobility in the distal leaflet. However, attempts to directly distinguish diffusivities in the two leaflets in a single measurement are bound to fail as diffusion time scales τ_D that differ by less than one order of magnitude cannot be disentangled given the data noise.

Similar measurements were performed on stBLMs and dtBLMs based upon FC16. Comprehensive results from the diffusion measurements for DOPC bilayers are compiled in Table 2.

4. Diffusivity of LR-DOPE in coexisting areas of distinct label solubility in DPhyPC

Optical inhomogeneities as those shown in Fig. 3b and d are not only associated with the deterioration of electrochemical characteristics but also with differences in dynamic properties of the bilayer. We measured the diffusivity of LR-DOPE in stBLMs showing lateral optical inhomogeneity in fluorescence micrographs. In these experiments, the stBLM was imaged in the LSM 510. Extended spots (diameters, $d > 5$ μm) of distinct fluorescence intensities were then selected and FC spectra determined near the centers of these spots. Fig. 6 shows a fluorescence micrograph (panel a) and corresponding FCS data (panel b) obtained for a DPhyPC stBLM prepared on FC16. Darker domains within the bilayer (such as spot 1 in panel a)

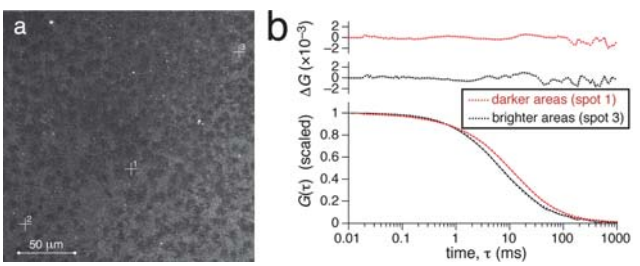

Fig. 6 (a) Fluorescence micrograph of a DPhyPC stBLM prepared on FC16/βME (30 : 70) with LR-DOPE (0.003 mol%). Scale bar is 50 μm. The contrast in the original image has been linearly enhanced. (b) FCS data were obtained at locations 1 and 3 indicated in panel (a). The original data, fits and residuals shown in the upper section of panel (b) were all scaled to the same values of $G(\tau \rightarrow 0)$. While the data obtained in spot 3 (brighter area) were well fitted with the model described by eqn (1), the data obtained in spot 1 (darker area) showed an uneven distribution of their residuals if fitted to eqn (1). They have therefore been fitted with two components of which the slow component ($\tau_D \approx 11.75$ ms) dominates the correlation decay (92% of the total amplitude). The fast component ($\tau_D \approx 0.43$ ms) might derive from 3D lipid aggregates, such as those seen in low abundance in panel (a), that adhere to the surface of the bilayer and diffuse along its surface through the buffer phase.

are less fluid ($D = 1.3 \pm 0.2$ μm^2 s^{-1}) than brighter fluorescent regions (such as spot 3), where $D = 4.0 \pm 0.5$ μm^2 s^{-1} (panel b).

IV. Discussion

The fluidity of biological membranes tightly packed with integral and peripheral proteins[35–37] deviates naturally from that of protein-free phospholipid bilayers. In fact, the patchiness in local composition of biomembranes resulting from their molecular heterogeneity leads to confined motion,[38] anomalous diffusivity and/or directional motion. Nevertheless, while biomembranes may display very distinct diffusion properties compared to pure phospholipid bilayers, it remains important to quantify the dynamics in tBLM systems, because these properties will affect protein reconstitution and molecular interactions within the bilayer. In this context, it has been recently reported that label diffusivity in DOPC bilayers supported by solid substrates is substantially lower than in free membranes.[2] However, these measurements did not discriminate between the inner and outer lipid leaflet of the supported membrane. Also, the bilayers were physisorbed to mica or glass surfaces, *i.e.*, it was not established whether the membrane was decoupled from the substrate by a thin water layer.

Tethered bilayer lipid membranes, such as the dtBLMs and stBLMs characterized in this study, are an emerging vehicle for biophysical studies of molecular interactions in basic and applied research. They comprise useful models for studies of membrane damage by amyloid-β peptide oligomers in Alzheimer's disease,[9] toxicology[15] and enzyme degradation.[19] We showed earlier that minute differences in their constitution may vastly alter the reactivity of enzymes targeting these membranes.[19] Inhomogeneities in the lateral organization of the bilayers such as a thickness reduction, in defect areas, of the hydration layer that separates the substrate from the membrane or, alternatively, phase separation into regions with distinct fluidity of acyl chains can alter their properties dramatically. It is therefore essential to identify preparation conditions which lead to fluid membranes with low defect density that resemble the lipid matrix in biological membranes closely. Phospholipid vesicles, a well-established model system proven in numerous biophysical studies, are the obvious benchmark for such comparisons.[39]

Neutron reflectivity provided indirect evidence that dtBLMs and stBLMs formed from phospholipids above their gel–fluid phase transition are uniform,[6,22] as such data are usually well accounted for by one unique neutron scattering length density profile across the bilayer.‡ Further circumstantial evidence for in-plane uniformity of the dtBLMs comes from EIS characterization that shows large resistivity to ion transfer ($\gg 100$ kΩcm^2) for bilayers composed of one phospholipid component, for example DPhyPC or DOPC. This would be hard to rationalize if there were inhomogeneities such as the coexistence of two phases, because phase boundaries constitute defect lines,§ likely promoting ion transfer. Beyond this indirect evidence, we show here directly (Fig. 2) that dtBLMs and stBLMs can be prepared to be uniform within the bilayer plane on the optical length scale.

Obtaining homogeneous tBLMs with rapid solvent exchange depends on careful control of the solvent-exchange procedure. We frequently observed heterogeneous bilayers, with morphologies reminiscent of phase-separated Langmuir monolayers, if the substrate was not fixed in the sample cell, such that turbulent flow around the vigorously agitated Si wafer occurred during the solvent-exchange step. Consistent with the conjecture that laminar flow in the solvent exchange promotes the formation of homogeneous bilayers, we note that low-resolution fluorescence images of stBLMs prepared in a closed flow cell, such as the one used for sample preparation for neutron studies,[40] also show homogeneous distribution of fluorescent labels (Frank Heinrich, personal communication). Conversely, samples for which the preparation conditions are less well-controlled show small-scale heterogeneities (Fig. 3), and here we show that the extent of inhomogeneity correlates with the electrical parameters determined in EIS.

In-plane heterogeneities such as those in Fig. 3d often show a bimodal distribution of the fluorescence intensities, similar to phase-separated Langmuir phospholipid monolayers. In Langmuir monolayers, it has been demonstrated that differences in fluorescence intensity derive from distinct solubilities of the lipid-bound label[41] in two coexisting thermodynamic phases,[42] the isotropic fluid L_E phase—termed L_α in bilayers—and the anisotropic fluid gel phase L_c,[43] equivalent to L_β. The two monolayer phases differ greatly in fluidity.[33,44] Similarly, it has been reported that the diffusivity in the fluid and gel phase in bilayers differs by approximately a factor of 20.[45] Although heterogeneities in the tBLMs are reminiscent of phase-separated monolayer domain structures, diffusivities in the two coexisting regions differ only by a factor of 2–4 (Fig. 6b), making it unlikely that the coexisting regions correspond to distinct thermodynamic phases with vastly different local chain order. Rather, it is likely that differences in the molecular constitutions of the coexisting areas are more subtle. For example, these areas might differ in the thickness of the hydration layer between membrane and substrate or in the local density of laterally intercalated phospholipids between the tether molecules in the proximal bilayer leaflet. Whatever the reason for the distinct label solubility, a recent study on GUVs also reported a situation in which the bilayers were organized into distinct domains with different solubilities for fluorescent labels which did not differ in their fluidity, as reported by EPR and PFG-NMR.[47] We also stress that the results reported in Fig. 4 and 5 were obtained on samples that were more homogeneous than those shown in Fig. 3 and 6. Indeed, Fig. 4c shows no indications of a bimodal distribution of the z-scan results. Measurement series data (not shown) for multiple samples of similar preparations were similarly distributed as the those in Fig. 4c.

The FCS measurements in this study establish that the molecular mobility of phospholipids in the distal leaflets of

‡ However, because a reflectivity experiment averages out-of-plane structures over large sample areas (of the order of cm^2 for neutron reflection), two coexisting phases with minor structural differences might be sufficiently well described by a model that averages these distinct structures. This is particularly true if the length scale of heterogeneities is below the in-plane coherence length of the neutron wave, as defined by the geometry and wavelength spread of the neutron experiment, which is typically on the order of μm.

§ For example, it has been shown that phase coexistence in floating surface monolayers promotes the action of phospholipase at the phase boundaries.[46]

tBLMs is similar to that in free bilayers such as those forming GUVs.[2,46] Moreover, the data match earlier results on physisorbed DOPC bilayers as well. The label diffusivity in DOPC stBLMs ($D \approx 4.1$ μm^2 s^{-1}) is only marginally above that in supported bilayers ($D = 3.5$ μm^2 s^{-1} at $T = 289$ K¶).[2] However, the picture that emerges from our results is more subtle.

1. Label diffusivities in distinct membrane leaflets

We have differentiated the diffusivities in the proximal and distal leaflets in the bilayer with different labeling schemes. Not surprisingly, they differ substantially. Due to the interaction of the labeled phospholipid with the tether molecules, the value $D = 2.0$ μm^2 s^{-1} in the proximal leaflet is significantly lower than that in free bilayers. The diffusion constant in the distal leaflet (~7.1 μm^2 s^{-1}), on the other hand, is similar to that reported for DOPC GUVs (6.3 μm^2 s^{-1} or 7.8 μm^2 s^{-1} in different reports[2,48]) or POPC‖ multi-bilayers (~5.5 μm^2 s^{-1} to ~6.3 μm^2 s^{-1}, depending on the label used).[49] The results provided in Table 2 are our best estimates for the diffusion constants in the leaflets proximal and distal to the substrate (columns 3 and 4, respectively), as well as the apparent diffusivities determined in membranes in which both leaflets contribute to the FCS signal (columns 2 and 5). In the latter case, the leaflet diffusivities are not discriminated as two distinct components in the correlation function $G(\tau)$ (see Fig. 4a), because they differ only by a factor of 4 and standard regularization cannot distinguish between components that differ by less than a factor of 10 because of the data noise. The results reported here for tBLMs differ substantially from similar measurements conducted on Langmuir–Blodgett deposited and vesicle-fused bilayers on quartz substrates and polymer-supported bilayers which all were reported to show the same diffusion properties (between differently prepared samples and within the proximal and distal leaflets) of $D = 2$–2.6 μm^2 s^{-1}.[30] This suggests that the proximal layer in those bilayer systems interacts substantially with the respective substrates, comparable to the interaction of tBLMs with the gold surface mediated by the covalently bound membrane anchors. Moreover, substantial transbilayer coupling is indicated by these results, which we do not observe in the tBLM samples investigated here. Transbilayer coupling has also been reported in polymer-tethered bilayers,[50] *i.e.*, membranes coupled to the support *via* substantially longer tethers that contained $n = 15$–85 ethylene glycol or oxazoline repeats, and this coupling has been attributed to corrugation of the bilayer induced by the membrane anchors *via* membrane deformations at the pinning sites. If such a scenario applies to the samples studied in the Granick group,[30] this might well account for the differences between their and our results, as we showed with neutron scattering that the substrates used for tBLM samples are atomically flat and the tethered bilayers are comparably smooth, with an rms roughness of $\sigma = 5$–6 Å between the distinct layers.[6,22] If corrugation of the bilayer contributes to transbilayer coupling, we would therefore not expect this mechanism to be relevant in our samples.

For a comparison of D values determined by distinguishing between the tBLM leaflets and those measured for the bilayer indiscriminately, we note that simple averaging is not appropriate. First, the label density is smaller in the proximal than in the distal leaflet of stBLMs due to the volume occupied by the tether. Therefore the contribution of labels in the proximal leaflet to $G(\tau)$ will be smaller. Secondly, while fluorescence quenching of the gold film is not too large to obtain measurements of reasonable signal-to-noise, quenching is expected to be more pronounced for labels in the proximal than for labels in the distal leaflet. On the other hand, the high ionic strength in the quenching experiments may influence the diffusivity. It has indeed been reported that D is decreased by a factor of ~3 in POPC bilayers upon increasing the buffer content of NaCl from 0 to 100 mM.[49] While we cannot estimate the concentration of KI in the submembrane space in the quenching experiments, it is likely much lower than in the bulk buffer due to the high resistance of the nearly defect-free tBLMs.[6] Nevertheless, we cannot entirely exclude that the reduction of the diffusion constant in the proximal leaflet is partially due to an increase in cation content in the hydrated bilayer cushion. Given these caveats it is indeed remarkable that for the case which we studied most extensively, DOPC on WC14, the apparent value of D is almost exactly the average of the values determined for the distal and proximal leaflets. Therefore until more rigorous metrologies of membrane fluidity emerge, we conclude that the D values determined with FCS for the bilayer indiscriminate of its individual leaflets are indeed a relevant measure of the dynamic properties of stBLMs.

2. Label diffusivities as a function of lipid composition

Consistent with the assumption that the apparent D value for stBLMs in which both leaflets are labeled is a representative measure of bilayer dynamics, diffusivity results for DPhyPC-based stBLMs are systematically lower than those for DOPC-based stBLMs. This can be reasonably expected, as DPhyPC is known to form densely packed bilayer cores while DOPC bilayers are more disordered due to their unsaturated chains. If this is the case, the molecular-scale interpretation of the numerical results in Table 2 is that lipid-bound label is more hindered in its mobility within the DPhyPC than in DOPC bilayers, possibly resulting from packing differences. We show here that FCS measurements of bilayer dynamics are sufficiently sensitive to quantify such minute differences.

3. Bilayer dynamics in WC14 and FC16-based stBLMs

Under otherwise identical conditions, we also observe slight differences between the label diffusivities in tethered bilayers based upon WC14 and FC16: D is lower in FC16-based tBLMs, even if only the distal bilayer leaflet is labeled (Table 2). Various differences between the molecular constitutions of the tether lipids and resulting differences in their organization at the solid substrate surface can contribute to the differences in bilayer dynamics. WC14 and FC16 differ both in the length of their hydrophilic oligo(ethyleneoxide) chains ($n = 6$ repeats in WC14 *vs.* $n = 9$ in FC16) and in the length of their polymethylene chains (R = $C_{14}H_{27}$ *vs.* $C_{16}H_{31}$). Just as the denser packing of diphytanoyl chains in DPhyPC bilayers decreases the mobility of

¶ Depending on the molecular label structure, Przybylo's results vary by ±0.3 μm^2 s^{-1}; for a comparison, we use their result for that label, Bodipy-FL-DHPE, which resembles most closely the LR-DOPE used in this work.

‖ POPC: 1- palmitoyl-2-oleoyl-*sn*-glycero-3-phosphocholine.

lipid-bound fluorescent labels, it is straightforward to assume that a similar effect will reduce the diffusivity of free lipids in the proximal bilayer leaflet of FC16 from that expected for WC14. Indeed, the increase in the polymethylene chain length increases the van der Waals interaction between chains. For example, an increase in hydrophobic chain length by two methylenes in phospholipid vesicles, *e.g.* containing DPPC *vs.* DMPC**, leads to an increase in the chain melting temperature by ~20 °C. From the enhanced interchain interaction between the tether lipid and intercalated free phospholipid, a reduction in the apparent diffusion constant determined for stBLMs in which both leaflets contain labeled lipid is to be expected, as seen in columns 2 and 5 of Table 2, even if only labels intercalated in the proximal bilayer leaflet might be substantially reduced in their mobility. Unexpected by this argumentation is the large magnitude of the label retardation which is ~50% of the retardation observed for DPhyPC lipid in comparison with DOPC. Table 2 shows that the reduction in D in a DOPC membrane is ~0.5 $\mu m^2 s^{-1}$ if FC16 is used as a tether lipid instead of WC14, while D changes by 1.0 $\mu m^2 s^{-1}$ if stBLMs are completed by DPhyPC instead of DOPC (both on WC14). Moreover, a difference of D values in dtBLMs based upon the two compounds is even observed (column 4) for the situation where the fluorescent label has only minimal direct interaction with the tether lipid.

A reasonable explanation of these results is that there is some residual intercalation of labeled phospholipid into the proximal leaflet even in dtBLMs, and that this residual intercalation is more pronounced for FC16 than for WC14. This is indeed feasible because the extended length of the oligo(ethylene oxide) head group in FC16 may lead to a more flexible organization of the tether lipid at the interface prior to reconstitution of the tBLM with free phospholipid. Not only would the intercalation of labeled phospholipid into the proximal layer explain the reduction in the apparent diffusion constant in dtBLMs, but it would also likely lead to a higher concentration of the label in the proximal leaflet of stBLMs based upon FC16, where the reduced label mobility will skew the apparent diffusivity observed as the sum of a faster component (distal leaflet) and a slower component (proximal leaflet) toward smaller apparent D values. Alternate scenarios, such as a topology-derived coupling between the two distinct bilayer leaflets discussed for tethered bilayers on much longer tether polymers,[50] are probably irrelevant to the situation discussed here, where the oligo(ethylene oxide) spacer is merely 9 repeat units long.

4. Small diffusivity differences in distinct regions of optically inhomogeneous bilayers

If bilayers are heterogeneous in appearance, as determined by fluorescence microscopy, then the diffusivities in coexisting regions are still comparable, usually within a factor of 2–4. This suggests that differences in the molecular organization of these distinct regions are minor. Would they be due to distinct lipid phases such as the fluid L_α phase and a hexatic (gel) phase, one would expect difference in the diffusivities much in excess of a factor of 10. For example, diffusion measurements using fluorescence recovery after photobleaching (FRAP) on vesicle membranes composed of phosphatidylcholines of various chain compositions show that the diffusivity in DMPC is ~25× greater than in DSPC at 300 K.[45] Because of the different length of the acyl chains on DMPC and DSPC††, this reflects the differences in label mobility which one expects in a system of coexisting fluid and gel phases. Here, we observe that the difference in D is an order of magnitude smaller in the optically distinct regions within tBLMs. We conclude that the bilayer within the tBLM is in a fluid phase state irrespective of the lateral imperfections, just as both the distal and proximal leaflets are in a fluid phase, even though D is significantly reduced in the proximal layer.

A possible interpretation of the distinct appearance of the coexisting regions within the stBLM shown in Fig. 6a is that these regions differ slightly in the composition or the thickness of their submembrane space, *i.e.*, of the hydrated layer that separates the bilayer from the solid substrate. If there was a difference in spacing by a fraction of a nanometre, this could be easily missed in the reflectivity characterization of the stBLM structure. However, a locally reduced distance between the fluorescently labeled membrane and the gold film will increase fluorescence quenching of the label, thereby reducing the emission intensity in those areas. Diffusivity might be affected by enhanced molecular interactions, and thereby increased effective viscosity, in areas of closer proximity of the membrane to the substrate. While this is speculative at this point, we suggest that the quantitative measurement and a more refined analysis of dynamic membrane properties can be used to characterize fine structural details that are not amenable to direct structural probes.

V. Conclusions

The calibration-free z-scan mode of measuring FCS data[25] is the method of choice for the study of bilayers such as those investigated here. In combination with maximum-likelihood error estimates based on multiple measurements of similarly prepared samples, we were able to determine diffusivities in tBLMs with very high precision.

We observed that the label diffusivity in the distal bilayer leaflet ($D \approx 7$ $\mu m^2 s^{-1}$ for DOPC) is indistinguishable from that in free lipid membranes such as those in GUVs. This suggests that both stBLMs and dtBLMs are systems that may be very well suited as a proxy to study the peripheral interaction of ligands with biomembranes. For example, peripheral membrane proteins would encounter molecular interactions that mimic those on free membranes. In distinction, label mobility in the proximal leaflet in stBLMs is significantly reduced ($D \approx 2$ $\mu m^2 s^{-1}$ for DOPC). However, the reduction in mobility is substantially less than that in bilayers that are irreversibly adsorbed to the substrate. A diffusion constant of ~2 $\mu m^2 s^{-1}$ still implies significant molecular mobility, and it is reasonable to assume that the label diffusion is just restricted by frequent collisions with the immobilized lipid anchor molecules. This conclusion is supported by neutron reflection measurements which showed that the proximal lipid leaflet is indeed separated by a nanometre thick hydration layer from the substrate[6,22] and by the observation that exotoxins, such as *S. aureus* α-hemolysin, incorporate readily

** DPPC: 1,2- dipalmitoyl-*sn*-glycero-3-phosphocholine; DMPC: 1,2-dimyristoyl-*sn*-glycero-3-phosphocholine.

†† DSPC: 1,2-distearoyl-*sn*-glycero-3-phosphocholine.

into the membrane, penetrating both the distal and proximal bilayer leaflets.[15]

The precision of the diffusivity measurements allowed systematic studies as a function of membrane architecture and showed that both the molecular identity of the lipidic anchor and the phospholipid filler affect the dynamic properties of the membrane. We thus demonstrated that DPhyPC stBLMs and dtBLMs show systematically smaller diffusivities than DOPC-based tBLMs. Surprisingly, there are also small but reproducible differences between the label diffusivities in tBLMs based upon WC14 and FC16. Our interpretation of those results is that a more malleable tether moiety on FC16 leads to residual incorporation of diffusible lipids into the proximal bilayer leaflet even in dtBLMs which, however, are expected to diffuse at a much lower rate than those in the distal leaflet. This would result in a reduced apparent value of D in comparison with a similarly prepared dtBLM based on WC14, which is expected to prevent more completely the incorporation of free lipid into its more rigid proximal leaflet.

Appendix: maximum-likelihood error estimates

Two different errors enter the N measurements D_i of the lipid diffusion constant. First, fitting the FCS signal yields a (known) variance, σ_i^2. Second, micro-heterogeneities within tBLMs and variability between tBLM samples imply variations in the diffusion constant independent of the FCS measurement accuracy, and we describe these by a variance, σ^2. Assuming both the distributions of measurement errors and sample preparation variations to be Gaussian, the probability density of finding some value D_i for the diffusion constant during measurement i is a Gaussian with mean D (the "true" diffusion constant) and variance $\sigma_i^2 + \sigma^2$, written as $G(D_i - D, \sigma_i^2 + \sigma^2)$. The probability density of measuring diffusion constants, D_1, D_2,…, D_N, with respective fitting errors, σ_1^2, σ_2^2,…, σ_N^2, in N measurements is then given by the likelihood function:

$$L\left(\{D_i\},\{\sigma_i\};D,\sigma^2\right)=\prod_{i=1}^{N}G\left(D_i-D,\sigma_i^2+\sigma^2\right) \qquad \text{(A1)}$$

The two unknown parameters D and σ^2 can be determined as maximum-likelihood estimators that maximize L at a given set of measurements, so the two equations $\partial L/\partial D = 0$ and $\partial L/\partial \sigma^2 = 0$ must hold. The first one can be solved for D as a function of σ^2:

$$D\left(\sigma^2\right)=\sum_{i=1}^{N}\frac{D_i}{\sigma_i^2+\sigma^2}\Bigg/\sum_{i=1}^{N}\frac{1}{\sigma_i^2+\sigma^2} \qquad \text{(A2)}$$

The second equation leads to the condition:

$$\sum_{i=1}^{N}\frac{(D_i-D)^2-\left(\sigma_i^2+\sigma^2\right)}{\left(\sigma_i^2+\sigma^2\right)}=0 \qquad \text{(A3)}$$

Upon inserting $D(\sigma^2)$ from eqn (A2), the left hand side of eqn (A3) becomes a function of the single unknown sample variance σ^2, for which we can solve numerically. Inserting this back into eqn (A2) we find the mean diffusion coefficient, D. Take note that in the special case where all σ_i^2 vanish, eqn (A2) and (A3) lead to the usual maximum-likelihood estimators for mean and variance of a distribution that we have sampled with N measurements. As is well known,[51] the estimator for the mean is unbiased, while the one for variance is only asymptotically unbiased.

The error in D is determined *via* error propagation:

$$(\delta D)^2=\sum_{i=1}^{N}\frac{\partial D}{\partial D_i}(\delta D_i)^2=\sum_{i=1}^{N}\frac{\partial D}{\partial D_i}\left(\sigma_i^2+\sigma^2\right) \qquad \text{(A4)}$$

Using eqn (A2) and some algebra, the partial derivative $\partial D/\partial D_i$ can be expressed as:

$$\frac{\partial D}{\partial D_i}=\frac{1}{\sum_{l=1}^{N}\frac{\sigma_i^2+\sigma^2}{\sigma_l^2+\sigma^2}}+\frac{\partial\sigma^2}{\partial D_i}\frac{\sum_{j=1}^{N-1}\sum_{k=j+1}^{N}\frac{\left(D_j-D_k\right)\left(\sigma_j^2-\sigma_k^2\right)}{\left(\sigma_j^2+\sigma^2\right)\left(\sigma_k^2+\sigma^2\right)}}{\left(\sum_{l=1}^{N}\frac{1}{\sigma_l^2+\sigma^2}\right)} \qquad \text{(A5)}$$

Lacking an analytical expression for σ^2, the second term $\partial\sigma^2/\partial D_i$ is difficult to handle. However, it multiplies an expression which is small, since $D_i \approx D_k$ and $\sigma_j^2 \approx \sigma_k^2$. To keep things simple, we approximate $\partial D/\partial D_i$ by only the first term in eqn (A5). This readily leads to the approximate error estimate:

$$\frac{1}{(\delta D)^2}=\sum_{i=1}^{N}\frac{1}{\sigma_i^2+\sigma^2} \qquad \text{(A6)}$$

Notice that the inverse errors add. Again, in the simple case where all σ_i^2 vanish, this reduces to the expected maximum-likelihood result, $\delta D \approx \sigma/N$. We mention in passing that the relative magnitudes of σ_i^2 and σ^2 provide a hint for experimental improvement: if σ^2 dominates, then sample preparation limits the overall accuracy and warrants improving, while a dominance of σ_i^2 suggests that the statistics of the measurement need to be increased.

Acknowledgements

This work is supported by the National Institute of Health (NIH) under (1 P01 AG032131) and the American Health Assistance Foundation (AHAF) under grant no. A2008-307. We thank Martin Hof and Aleš Benda for valuable advice on practical aspects of the FCS measurements and Frank Heinrich for critically reading the manuscript.

References

1 B. A. Cornell, V. L. B. Braach-Maksvytis, L. B. King, P. D. J. Osman, B. Raguse, L. Wieczorek and R. J. Pace, *Nature*, 1997, **387**, 580–583.
2 M. Przybylo, J. Sýkora, J. Humpolíckova, A. Benda, A. Zan and M. Hof, *Langmuir*, 2006, **22**, 9096–9099.
3 L. K. Tamm and H. M. McConnell, *Biophys. J.*, 1985, **47**, 105–113.
4 E. Kalb, S. Frey and L. K. Tamm, *Biochim. Biophys. Acta*, 1992, **1103**, 307–316.
5 H. M. McConnell, L. K. Tamm and R. M. Weis, *Proc. Natl. Acad. Sci. U. S. A.*, 1984, **81**, 3249–3253.
6 D. J. McGillivray, G. Valincius, D. J. Vanderah, W. Febo-Ayala, J. T. Woodward, F. Heinrich, J. J. Kasianowicz and M. Lösche, *Biointerphases*, 2007, **2**, 21–33.
7 A. Schmidt, J. Spinke, T. Bayerl, E. Sackmann and W. Knoll, *Biophys. J.*, 1992, **63**, 1185–1192.
8 I. D. Raistrick, D. R. Franceschetti and J. R. Macdonald, in *Impedance Spectroscopy: Theory, Experiment, and Applications*, ed. E. Barsoukov and J. R. Macdonald, Wiley, New York, 2005, pp. 27–117.
9 G. Valincius, F. Heinrich, R. Budvytyte, D. J. Vanderah, D. J. McGillivray, Y. Sokolov, J. E. Hall and M. Lösche, *Biophys. J.*, 2008, **95**, 4845–4861.

10 E. Sackmann, *Science*, 1996, **271**, 43–48.
11 M. Tanaka and E. Sackmann, *Nature*, 2005, **437**, 656–663.
12 M. Tanaka, *MRS Bull.*, 2006, **31**, 513–520.
13 I. K. Vockenroth, C. Ohm, J. W. F. Robertson, D. J. McGillivray, M. Lösche and I. Köper, *Biointerphases*, 2008, **3**, FA68–FA73.
14 I. K. Vockenroth, P. P. Atanasova, A. T. A. Jenkins and I. Köper, *Langmuir*, 2008, **24**, 496–502.
15 D. J. McGillivray, G. Valincius, F. Heinrich, J. W. F. Robertson, D. J. Vanderah, W. Febo-Ayala, I. Ignatjev, M. Lösche and J. J. Kasianowicz, *Biophys. J.*, 2009, **96**, 1547–1553.
16 O. Purrucker, A. Förtig, R. Jordan, E. Sackmann and M. Tanaka, *Phys. Rev. Lett.*, 2007, **98**, 078102.
17 H. M. Keizer, B. R. Dorvel, M. Andersson, D. Fine, R. B. Price, J. R. Long, A. Dodabalapur, I. Köper, W. Knoll, P. A. V. Anderson and R. S. Duran, *ChemBioChem*, 2007, **8**, 1246–1250.
18 R. Robelek, E. S. Lemker, B. Wiltschi, V. Kirste, R. Naumann, D. Oesterhelt and E. K. Sinner, *Angew. Chem., Int. Ed.*, 2007, **46**, 605–608.
19 G. Valincius, D. J. McGillivray, W. Febo-Ayala, D. J. Vanderah, J. J. Kasianowicz and M. Lösche, *J. Phys. Chem. B*, 2006, **110**, 10213–10216.
20 H. Song, E. K. Sinner and W. Knoll, *Biointerphases*, 2007, **2**, 151–158.
21 S. A. Glazier, D. J. Vanderah, A. L. Plant, H. Bayley, G. Valincius and J. J. Kasianowicz, *Langmuir*, 2000, **16**, 10428–10435.
22 F. Heinrich, T. Ng, D. J. Vanderah, P. Shekhar, M. Mihailescu, H. Nanda and M. Lösche, *Langmuir*, 2009, **25**, 4219–4229.
23 D. Magde, W. W. Webb and E. Elson, *Phys. Rev. Lett.*, 1972, **29**, 705–708.
24 A. J. Garcia-Saez and P. Schwille, *Methods*, 2008, **46**, 116–122.
25 A. Benda, M. Benes, V. Marecek, A. Lhotsky, W. T. Hermens and M. Hof, *Langmuir*, 2003, **19**, 4120–4126.
26 E. Haustein and P. Schwille, *Annu. Rev. Biophys. Biomol. Struct.*, 2007, **36**, 151–169.
27 E. Haustein and P. Schwille, *Methods*, 2003, **29**, 153–166.
28 S. M. Sorscher and M. P. Klein, *Rev. Sci. Instrum.*, 1980, **51**, 98–102.
29 P. Schwille, U. Haupts, S. Maiti and W. W. Webb, *Biophys. J.*, 1999, **77**, 2251–2265.
30 L. F. Zhang and S. Granick, *J. Chem. Phys.*, 2005, **123**, 211104.
31 C. Rossi and J. Chopineau, *Eur Biophys. J.*, 2007, **36**, 955–965.
32 A. R. Sapuri-Butti, Q. Li, J. T. Groves and A. N. Parikh, *Langmuir*, 2006, **22**, 5374–5384.
33 M. Lösche, E. Sackmann and H. Möhwald, *Ber. Bunsen-Ges. Phys. Chem.*, 1983, **87**, 848–852.
34 P. Krüger and M. Lösche, *Phys. Rev. E: Stat. Phys., Plasmas, Fluids, Relat. Interdiscip. Top.*, 2000, **62**, 7031–7043.
35 D. M. Engelman, *Nature*, 2005, **438**, 578–580.
36 R. Phillips, T. Ursell, P. Wiggins and P. Sens, *Nature*, 2009, **459**, 379–385.
37 S. Takamori, M. Holt, K. Stenius, E. A. Lemke, M. Grønborg, D. Riedel, H. Urlaub, S. Schenck, B. Brügger, P. Ringler, S. A. Müller, B. Rammner, F. Gräter, J. S. Hub, B. L. de Groot, G. Mieskes, Y. Moriyama, J. Klingauf, H. Grubmüller, J. Heuser, F. Wieland and R. Jahn, *Cell*, 2006, **127**, 831–846.
38 A. Kusumi, C. Nakada, K. Ritchie, K. Murase, K. Suzuki, H. Murakoshi, R. Kasai, J. Kondo and T. Fujiwara, *Annu. Rev. Biophys. Biomol. Struct.*, 2005, **34**, 351–378.
39 L. Guo, J. Y. Har, J. Sankaran, Y. Hong, B. Kannan and T. Wohland, *ChemPhysChem*, 2008, **9**, 721–728.
40 J. A. Dura, D. Pierce, C. F. Majkrzak, N. Maliszewskyj, D. J. McGillivray, M. Lösche, K. V. O'Donovan, M. Mihailescu, U. A. Perez-Salas, D. L. Worcester and S. H. White, *Rev. Sci. Instrum.*, 2006, **77**, 074301.
41 M. Lösche and H. Möhwald, *Eur. Biophys. J.*, 1984, **11**, 35–42.
42 A. Miller, W. Knoll and H. Möhwald, *Phys. Rev. Lett.*, 1986, **56**, 2633–2636.
43 D. A. Cadenhead, F. Müller-Landau and B. M. J. Kellner, in *Ordering in Two Dimensions*, ed. S. K. Sinha, Elsevier, North Holland, Amsterdam, 1980, pp. 73–81.
44 R. Peters and K. Beck, *Proc. Natl. Acad. Sci. U. S. A.*, 1983, **80**, 7183–7187.
45 V. Schram, H. N. Lin and T. E. Thompson, *Biophys. J.*, 1996, **71**, 1811–1822.
46 D. W. Grainger, A. Reichert, H. Ringsdorf and C. Salesse, *Biochim. Biophys. Acta*, 1990, **1023**, 365–379.
47 J. B. de la Serna, G. Orädd, L. A. Bagatolli, A. C. Simonsen, D. Marsh, G. Lindblom and J. Perez-Gil, *Biophys. J.*, 2009, **97**, 1381–1389.
48 N. Kahya, D. Scherfeld, K. Bacia and P. Schwille, *J. Struct. Biol.*, 2004, **147**, 77–89.
49 R. A. Böckmann, A. Hac, T. Heimburg and H. Grubmüller, *Biophys. J.*, 2003, **85**, 1647.
50 M. Deverall, S. Garg, K. Lüdtke, R. Jordan, J. Rühe and C. A. Naumann, *Soft Matter*, 2008, **4**, 1899.
51 D. S. Sivia and J. Skilling, *Data Analysis—A Bayesian Tutorial*, Oxford University Press, Oxford, 2006.

